Characterization of the RFX Complex and the RFX5(L66A) Mutant: Implications for the Regulation of MHC Class II Gene Expression†

Colin W. Garvie,*,§ Jason R. Stagno,§ Sarah Reid,§ Ashina Singh,§ Erik Harrington,§ and Jeremy M. Boss‖

Department of Chemistry and Biochemistry, University of Maryland Baltimore County, 1000 Hilltop Circle, Baltimore, Maryland 21250, and Department of Microbiology and Immunology, Emory University School of Medicine, 1510 Clifton Road, Atlanta, Georgia 30322

Received November 17, 2006

ABSTRACT: Major histocompatability complex class II (MHCII) molecules are an essential component of the mammalian adaptive immune response. The expression of MHCII genes is regulated by a cell-specific multiprotein complex, termed the MHCII enhanceosome. The heterotrimeric RFX complex is the key DNA-binding component of the MHCII enhanceosome. The RFX complex is comprised of three proteins, RFXB, RFXAP, and RFX5, all of which are required for DNA binding and activation of MHCII gene expression. Static light scattering and chemical cross-linking of the three RFX proteins show that RFXB and RFXAP are monomers and that RFX5 dimerizes through two separate domains. One of these domains, the oligomerization domain, promotes formation of a dimer of dimers of RFX5. In addition, we show that the RFX complex forms a 2:1:1 complex of RFX5·RFXAP·RFXB, which can associate with a further dimer of RFX5 to form a 4:1:1 complex through the oligomerization domain of RFX5. On the basis of these studies, we propose DNA-binding models for the interaction between the RFX complex and the MHCII promoter including a DNA looping model. We also provide direct evidence that the RFX5(L66A) point mutation prevents dimerization of the RFX complexes and propose a model for how this results in a loss of MHCII gene expression.

The human adaptive immune system serves as the primary defense against a host of pathogenic bacteria, viruses, and fungi. The major histocompatability class II (MHCII)[1] molecules have a central role in the initiation of this immune response (*1*). MHCII molecules are heterodimeric glycoproteins that present antigens on the surface of antigen-presenting cells such as B-cells, macrophages, and dendritic cells. The interaction of the MHCII−antigen complex with CD4+ T cells leads to T cell activation, differentiation, and proliferation. There is a direct correlation between the level of expression of MHCII molecules in antigen-presenting cells and the ability of the immune system to mount a response against infection. This correlation is highlighted in the bare lymphocyte syndrome (BLS), a severe immunodeficiency disorder characterized by a lack of expression of MHCII genes (*2*).

There are three MHCII isotypes expressed in humans. The promoters of the genes that code for the MHCII isotypes contain four highly conserved DNA sequences, the S-box, the X1-box, the X2-box, and the Y-box, all of which are required for efficient regulation of expression of the MHCII genes (*3*, *4*). A highly specific multiprotein complex was identified to assemble on the MHCII promoters and regulate expression of the MHCII genes in a cell-specific manner. The term "enhanceosome" has been used to represent multiprotein complexes that regulate the expression of eukaryotic genes (*5*, *6*), and thus this complex has been described as the MHCII enhanceosome.

The X1-box sequence and, potentially, the S-box sequence are bound by the heterotrimeric RFX complex. The RFX complex is comprised of three proteins: RFX5, RFXB, and RFXAP (Figure 1A). All three proteins are required to obtain high-affinity binding to the X1-box sequence and to recruit the other components of the MHCII enhanceosome (*7*−*10*). The importance of the RFX proteins is highlighted in the BLS. Patients suffering from BLS are classified into four complementation groups: A, B, C, and D. Groups B, C, and D are characterized by point mutations or deletions in RFXB, RFX5, and RFXAP, respectively (*11*−*16*).

RFX5 is the fifth member of a small family of mammalian transcription factors that share sequence homology in their DNA-binding domain (*17*). RFX5 can be separated into five distinct regions: the oligomerization domain, the RFX DNA-binding domain, the helical domain, the proline-rich region, and the transactivation domain (Figure 1A). The oligomerization domain, residues 1−90, has two distinct roles in RFX

† This work was supported by internal research grants at the University of Maryland Baltimore County.

* To whom correspondence should be addressed. Telephone: (410) 455-2512. Fax: (410) 455-2608. E-mail: garvie@umbc.edu.

§ University of Maryland Baltimore County.

‖ Emory University School of Medicine.

[1] Abbreviations: MHCII, major histocompatability complex class II; DTT, dithiothreitol; IPTG, isopropyl β-D-thiogalactopyranoside; CBD, chitin binding domain; TEV, tobacco etch virus; HTT, six histidine affinity tag with TEV cleavage site; EDC, 1-ethyl-3-[3-(diethylamino)propyl]carbodiimide hydrochloride; NHS, *N*-hydroxysuccinimide; SDS−PAGE, sodium dodecyl sulfate−polyacrylamide gel electrophoresis; SEC-SLS, size exclusion chromatography with static light scattering; MALDI-TOF, matrix-assisted laser desorption/ionization time of flight; SE, sedimentation equilibrium.

10.1021/bi6023868 CCC: $37.00
Published on Web 01/20/2007

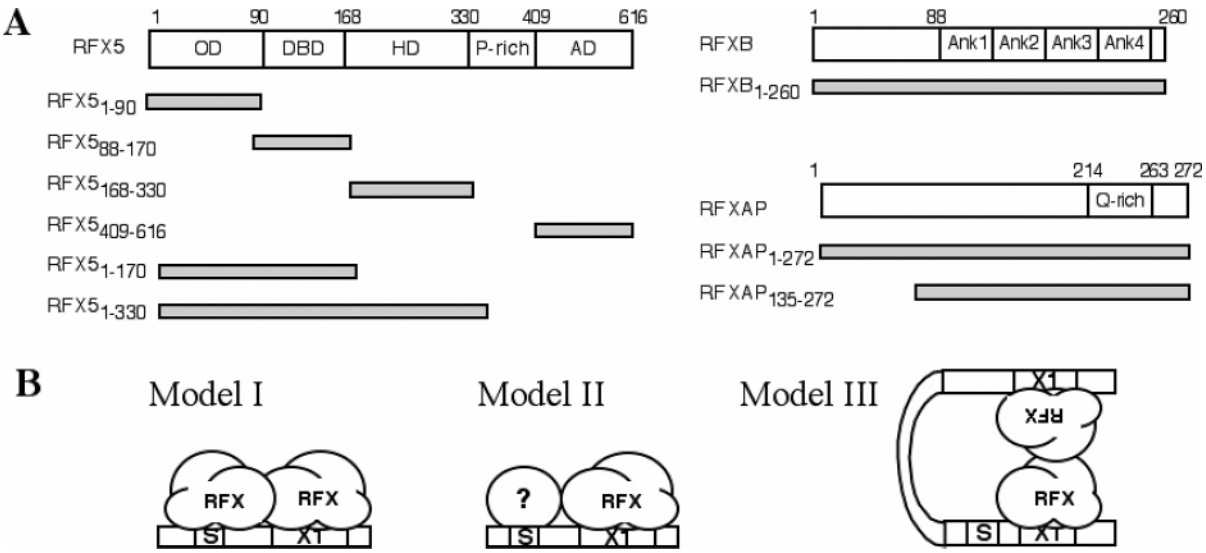

FIGURE 1: Summary of the RFX protein domains and how the RFX complex interacts with DNA. (A) Schematics of the RFX protein domain structures and the constructs expressed. For RFX5, OD stands for oligomerization domain, DBD stands for the RFX DNA-binding domain, HD stands for helical domain, P-rich refers to the proline-rich region, and AD stands for the activation domain. For RFXB, Ank represents an ankyrin repeat. For RFXAP, Q-rich represents the glutamine-rich region. (B) Models for the interaction of the RFX complex with DNA. Model I: Two RFX complexes binding cooperatively to the S-box and X1-box. Model II: One RFX complex bound to the X1-box and an unknown factor bound to the S-box. Model III: Two RFX complexes bound to the proximal and distal X1-box sequence.

complex assembly. It mediates dimerization between RFX complexes, which is important for binding to the MHCII promoter (*18*, *19*), and it encompasses the primary region of RFX5 that interacts with RFXB and RFXAP (*20*). Chemical screening for point mutations of RFX5 that inhibited MHCII gene expression identified the importance of a leucine-rich region between residues 62 and 68 in the oligomerization domain (*18*). A single point mutation within this region, RFX5(L66A), inhibited DNA binding without preventing assembly of the RFX complex (*19*). The RFX DNA-binding domain of RFX5, hereafter referred to as the RFX5-RFX domain, is the major DNA-binding component of the RFX complex. The RFX5-RFX domain is a member of the winged-helix subfamily of helix−turn−helix proteins (*21*). Residues 168−330 are predicted to form a helical structure from secondary structure predictions of the amino acid sequence. This region may be involved in interactions with RFXB, RFXAP, and other components of the MHCII enhanceosome (*20*; J. M. Boss, personal communication). The remainder of RFX5 comprises a proline-rich region and the transactivation domain, which are involved in activation of expression of the MHCII genes and contacting other proteins in the MHCII enhanceosome (*20*, *22*).

The second component of the RFX complex, RFXB, is a 260 amino acid protein that contains four ankyrin repeats (*23*). Ankyrin repeats are common protein−protein interaction motifs and have been found in numerous proteins (*24*). The ankyrin repeats of RFXB are essential for assembly and for DNA binding of the RFX complex (*2*, *20*, *23*, *25*, *26*).

The final component of the RFX complex, RFXAP, is a 272 amino acid protein that shows no sequence homology with proteins of known structure. RFXAP interacts with both RFXB and RFX5 through a glutamine-rich region at its C-terminus (*12*, *20*, *23*, *27*). Cross-linking studies of the RFX complex bound to DNA suggest that RFXAP is directly involved at the RFX−DNA-binding interface (*28*).

RFXAP can form a complex with RFX5 and RFXB individually, but it is not clear whether RFX5 can interact with RFXB in the absence of RFXAP (*19*, *20*, *25*, *27*, *29*). Recent studies have shown that RFX5 and RFXAP assemble in the cytoplasm prior to translocating into the nucleus, where they form the full RFX complex with RFXB (*30*).

Three models exist for the binding of the RFX complex to the MHCII promoter (Figure 1B). In the first model, two RFX complexes bind cooperatively to the S-box and the X1-box. This model is supported by the ability of the RFX complex to bind individually to both sites on the MHCII promoter and to be able to dimerize through the RFX5 oligomerization domains (*10*, *19*). In the second model, a single RFX complex binds to the X1-box, and an as yet unidentified factor binds to the S-box (*31*). This model is supported by experiments that show the same amount of the RFX complex is bound to the MHCII promoter even when the S-box is mutated. Recently, other (distal) X1-box sites that are potentially involved in regulating expression of the MHCII genes have been identified upstream of the (proximal) X1-box located closest to the transcription initiation site (*32*−*34*). Binding of RFX to the proximal X1-box and one of the distal X1-boxes induced looping of the DNA, leading to a third model for RFX interaction with the MHCII promoter (*34*).

All of the RFX proteins contact other components of the MHCII enhanceosome. The stoichiometry of the RFX complex will therefore have a direct impact on the assembly of the entire MHCII enhanceosome. The stoichiometry will also directly influence how the RFX complex will bind to the MHCII promoter. Previous attempts to determine the oligomeric states of RFX5 and the complexes it forms with RFXAP and RFXB have been complicated by the formation of multiple oligomeric states (*29*). We have characterized the oligomeric state of the RFX proteins and the stoichiometries of the complexes they form. From these studies, we propose models for assembly of the RFX complex on the MHCII promoter. We also show the effect of the RFX5-(L66A) point mutation on complex assembly and propose a model for how it prevents MHCII gene expression.

Table 1: Oligonucleotide Primers Used in PCR

primer name	sense/antisense	primer sequence (5′−3′)
RFXB-1-NCOI	sense	ATGGACCCCATGGAATGGAGCTTACCCAGCCTGCA
RFXB-260-BAMHI	antisense	GGCACGGAGGGATCCTCACTCAGGGTCAGCGGGCACCAG
RFXAP-1-NCOI	sense	ATGGACCCATGGAATGGAGGCGCAGGGTGTAGCG
RFXAP-135-NCOI	sense	GACTTACCATGGCAGCATGAGCAAGACC
RFXAP-272-BAMHI	antisense	AGTGACGGATCCTCACATTGATGTTCCTGGAAACTG
RFX5-1-BSPHI	sense	CGACTAGCATGAAGATGAGCCTGATGCT
RFX5-88-NCOI	sense	CAGTTACCATGGAGAGTACATGTATGCCTAT
RFX5-168-SFOI	sense	CACTGGAGGCGCCACCTTGGTGTCTATGCCA
RFX5-409-BAMHI	sense	CACTGACGGATCCCCGGGGCACAGAGAACAGA
RFX5-90-HINDIII	antisense	CACTGGAAAGCTTTTACATGTACTCCTCATTGCTCAG
RFX5-170-HINDIII	antisense	GGCACTGCCAAGCTTCACACCAAGGTCTTCCTCCTTAT
RFX5-330-HINDIII	antisense	CACTGGAAAGCTTTTAAGGCAGCCGAGCCACTAGGGC
RFX5-616-HINDIII	antisense	CACTGGAAAGCTTATGGGGGTGTTGCTTTTGGGTC
RFX5-L66A-1	sense	GACAAGCTGTATCTCTATGCGCAGCTCCCCTCAGGACCCACC
RFX5-L66A-2	antisense	GGTGGGTCCTGAGGGGAGCTGCGCATAGAGATACAGCTTGTC
T7 promoter	sense	TAATACGACTCACTATAG

MATERIALS AND METHODS

Construction of the RFX Protein Expression Vectors. PCR was performed on vectors containing full-length RFXB, RFXAP, and RFX5 (*20*). The constructs made are summarized in Figure 1A, and the primers used to PCR amplify the constructs are listed in Table 1. The PCR product for RFX5(168−330) was inserted into the pProExHT vector (Invitrogen), which attaches a 20 amino acid affinity tag (HTT) to the N-terminus of the inserted protein. This affinity tag is comprised of six histidines, a short linker, and a tobacco etch virus (TEV) protease cleavage site. The PCR products for the remaining RFX5 constructs and RFXB were inserted into the pHTCBD vector. The pHTCBD vector was constructed from the pET21a vector and encodes an N-terminal 70 amino acid affinity tag (HTCBD). The HTCBD affinity tag is comprised of six histidines, the chitin binding domain (CBD), and a TEV protease cleavage site. The primers were purchased from Integrated DNA Technologies (Coralville, IA). The PCR products were purified with the QIAquick PCR purification protocol (QIAGEN). After cleavage with the appropriate restriction enzymes (see Table 1), the PCR products and the vectors were purified by agarose gel electrophoresis and extracted from the gel using Geneclean (BIO101). DH5α cells were transformed with the ligated PCR product and vector and were plated onto an LB-agar plate containing 100 μg/mL carbenecillin. Colonies containing the PCR insert were identified by PCR screening with the T7 promoter primer and an antisense strand corresponding to the related insert (Table 1). Two colonies were transferred to 1 mL of LB/ampicillin growth media and grown for 12 h at 37 °C. Cell culture (1 mL) was used to inoculate 100 mL of LB/ampicillin media, which was grown for a further 14 h at 37 °C. Afterg the cells were harvested by centrifugation, the vectors were purified following the Midi-prep protocol (QIAGEN). The correct insertion of the PCR product was confirmed by DNA sequencing (Center for Biosystems Research at the University of Maryland College Park, MD). The RFXAP and RFXAP(135−272) PCR products were inserted into the vector pCBD in an identical manner as for the RFX5 proteins. pCBD differs from pHTCBD by the absence of the six histidine sequence N-terminal to the CBD.

Site-Directed Mutagenesis of RFX5. The L66A mutant was introduced into the relevant vectors using the QuikChange site-directed mutagenesis protocol (Stratagene). PCR was performed with the vectors encoding RFX5(1−90), RFX5-(1−170), and RFX5(1−330) using the RFX5-L66A-1 and RFX5-L66A-2 primers given in Table 1. In addition to introducing the L66A mutation into the RFX5 genes, the primers inserted an *Fsp*I restriction site. The PCR products were treated with *Dpn*I to degrade the parent plasmid prior to transforming DH5α cells. Colonies were screened for the presence of the point mutation by PCR amplification of the respective RFX5 gene followed by addition of *Fsp*I. Two of the colonies that showed cleavage of the PCR product by *Fsp*I were transferred to 1 mL of LB/ampicillin media and grown for 12 h. Extraction and purification of the vectors were performed as described for the wild-type proteins, and the presence of the mutation was confirmed by DNA sequencing.

Expression and Purification of RFX5 Fragments. The vectors encoding the RFX5 constructs were expressed in *Escherichia coli* under the control of the T7 promoter. BL21-(DE3) CodonPlus(DE3)-RP cells (Stratagene) were grown at 37 °C to mid-log phase before being induced with IPTG to a final concentration of 0.5 mM. The cells were grown for a further 3 h at 37 °C before being harvested by centrifugation. The cells were resuspended in lysis buffer that was comprised of 50 mM Tris buffer, pH 8.0, 500 mM NaCl, 50 mM imidazole, and 1 mM DTT and lysed with a microfluidizer (Microfluidics Corp., Newton, MA). The soluble protein was extracted by centrifugation followed by filtration with a 0.45 μm filter. All six protein constructs were initially purified by loading onto a nickel-charged HisTrap column (GE Healthcare) and eluting with a gradient of 0−1 M imidazole. After the eluted fractions were combined, the affinity tag was cleaved by addition of TEV protease and incubation for 5 h at room temperature. The protein was dialyzed to remove the imidazole and passed over the nickel-charged HisTrap column to remove the affinity tag and TEV protease, which contained an N-terminal polyhistidine sequence. RFX5(168−330) was further purified by dialyzing into 50 mM Tris, pH 8.0, 50 mM NaCl, and 1 mM DTT followed by loading onto a MonoQ cation-exchange column (GE Healthcare). RFX5(409−616) was dialyzed into the same buffer but was loaded onto a MonoS anion-exchange column (GE Healthcare). The two proteins were eluted from their respective ion-exchange columns

using a 0−1 M gradient of NaCl. All of the proteins were dialyzed into 20 mM phosphate buffer, pH 7.0, 150 mM NaCl, and 1 mM DTT and then concentrated prior to loading onto a size exclusion column. RFX5(1−90), RFX5(1−90,-L66A), RFX5(88−170), and RFX5(409−616) were purified with a 16/60 Superdex 75 column (GE Healthcare). The remaining RFX5 constructs were purified with a 16/60 Superdex 200 column (GE Healthcare). The proteins were concentrated and stored at −20 °C until use.

Expression and Purification of RFXB. RFXB was expressed in an similar manner to the RFX5 constructs. Once the mid-log phase had been reached, the growth temperature was reduced to 30 °C, and the cells were induced for 3 h. The protein was lysed and purified with a nickel-charged HisTrap column as for the RFX5 proteins, except the lysis buffer contained 10 mM imidazole to ensure maximum binding of protein to the nickel column. The protein was further purified on a MonoQ column as described for RFX5-(168−330). RFXB was dialyzed into 20 mM phosphate buffer, pH 7.0, 150 mM NaCl, and 1 mM DTT and then concentrated prior to loading onto a 16/60 Superdex 75 column. RFXB was concentrated and stored at −20 °C until use.

Expression and Purification of RFXAP and RFXAP(135−272). The CBD-RFXAP fusion proteins were expressed in a similar manner to the RFX5 proteins except BL21(DE3)-pLysS cells (Stratagene) were used to optimize protein yield. Cells containing overexpressed CBD-RFXAP and HTCBD-RFX5(1−90) were resuspended in the lysis buffer described previously, and the cells were lysed with a microfluidizer. The two fusion proteins form a highly stable complex and were purified over a nickel-charged HisTrap column. After elution, urea was added to the combined fractions to give a final concentration of 6 M urea. The denatured protein was dialyzed to remove the imidazole and passed back over the nickel-charged HisTrap column under denaturing conditions in order to separate CBD-RFXAP and HTCBD-RFX5(1−90). CBD-RFXAP was refolded by reducing the concentration of urea to 0 M over a period of 2 days. Initially, the protein was diluted to 0.1−0.2 mg/mL before dialyzing into 3 M urea, 50 mM Tris, pH 8.0, 500 mM NaCl, 1 mM DTT, and 1 mM EDTA. After 6 h the protein was transferred to a similar solution but containing 2 M urea, 1 M urea, and finally 0 M urea. The affinity tag was cleaved by addition of TEV protease. The TEV protease was removed by passing the protein over a nickel-charged HisTrap column. RFXAP was dialyzed into 20 mM phosphate buffer, pH 7, 150 mM NaCl, and 1 mM DTT and concentrated prior to loading over a 16/60 Superdex 200 column. RFXAP(135−272) was expressed and purified in an identical manner to full-length RFXAP. Both proteins were stored at −20 °C until use.

SEC-SLS Studies of the RFX Proteins. SEC-SLS was performed using an AKTA purifier (GE Healthcare) with the following components: a size exclusion column, a Monitor UV-900 UV detector (GE Healthcare), a 0.2 μm online filter, and a miniDAWN tri-star light scattering detector (Wyatt Technologies, Santa Barbara, CA). A 10/30 Superdex 200 column was used for all proteins except for RFX5(1−330), RFX5(1−330,L66A), and the complexes they formed. In these cases, a 10/30 Superose 6 column was connected in series with a 10/30 Superdex 200 column. Size exclusion was performed at 0.2 mL/min with a running buffer of 20 mM phosphate buffer, pH 7.0, 150 mM NaCl, and 1 mM DTT. Two hundred microliters of between 50 μM and 0.5 mM protein was loaded onto the column after filtering with a 0.2 μm centrifugal spin filter. The concentrations of the proteins were calculated on the basis of the theoretical extinction coefficient at 280 nm for a monomer (*35*) (Table 2) and were chosen to optimize the static light scattering signal. As the protein eluted from the column, its absorbance at 280 nm was measured using the Monitor UV-900 detector, and the scattering of light was measured using the miniDAWN light scattering detector. The concentration of the protein was calculated using the absorbance at 280 nm and the theoretical extinction coefficient for the protein. The concentration was used together with the light scattering data to calculate the solution mass of the protein using the ASTRA software (Wyatt Technologies). The protein typically eluted with a peak width corresponding to 1−2 mL. Light scattering data were collected over this entire peak. For each data point on the peak, the solution mass was calculated. The final mass for each protein was determined as the average mass obtained over the entire eluted peak, which was typically comprised of at least 100 independently measured data points. The SEC-SLS experiments were repeated three times to obtain an accurate estimate of the solution mass.

Table 2: SEC-SLS Analysis of the RFX Proteins

protein	ϵ_{280} (M^{-1} cm^{-1})[a]	mass from SLS (kDa)[b]	oligomeric state (theoretical mass, kDa)[c]
RFXB(1−260)	23950	28.4 ± 0.4	monomer (28.4)
RFXAP(1−272)	11460	28.6 ± 1.0	monomer (28.5)
RFXAP(135−272)	9970	18.2 ± 0.4	monomer (15.8)
RFX5(1−90)	4470	33.3 ± 0.9	trimer (28.9)−tetramer (38.6)[d]
RFX5(1−90), cross-linked	4470	38.4 ± 0.4	tetramer (38.6)
RFX5(88−170)	17420	11.4 ± 0.7	monomer (10.1)
RFX5(168−330)	5500	31.8 ± 0.4	dimer (35.2)
RFX5(409−616)	16500	24.2 ± 0.5	monomer (22.2)
RFX5(1−170) peak 1	20400	72.7 ± 1.0	tetramer (76.3)
RFX5(1−170) peak 2	20400	50.9 ± 2.1	dimer (38.1)−trimer (57.2)[d]
RFX5(1−330) peak 1	25900	132.3 ± 7	tetramer (144.9)
RFX5(1−330) peak 2	25900	81.1 ± 0.3	dimer (72.4)
RFX5(1−90,L66A)	4470	17.9 ± 1.1	dimer (19.2)
RFX5(1−170,L66A)	20400	33.5 ± 1.5	dimer (38.2)
RFX5(1−330,L66A)	25900	73.9 ± 2.2	dimer (72.3)

[a] The theoretical extinction coefficient was calculated using the equation proposed by Pace et al. (*35*). [b] The solution mass and error were calculated from the results of at least three independent SEC-SLS experiments. [c] The theoretical mass was calculated on the basis of the number of polypeptide chains and the theoretical mass of a monomer. The theoretical mass of a monomer was calculated using the amino acid sequence. [d] These constructs gave observed masses between two oligomeric states (see text for discussion).

SEC-SLS Studies of the RFX Complexes. The experimental setup for SEC-SLS analysis of the RFX protein complexes was identical to that of the RFX proteins alone. To analyze complex formation between RFXB and RFXAP, as well as between the RFX5 constructs and RFXAP, each protein (100 μM), calculated on the basis of monomer concentration, was mixed in a 1:1 ratio, and 200 μL was loaded onto the size exclusion column. Excess of one or other of the two proteins

Table 3: SEC-SLS Analysis of the Complexes Formed by the RFX Proteins

complex	ratio	ϵ_{280} ($M^{-1}\,cm^{-1}$)[a]	theoretical mass (kDa)[b]	mass from SEC-SLS (kDa)[c]
RFXB·RFXAP	1:1	35910	56.8	41.7 ± 3.2
RFX5(1−90)·RFXAP	1:1	15930	38.1	40.2 ± 0.3
RFX5(1−90)·RFXAP·RFXB	1:1:1	39880	66.5	66.3 ± 2.3
RFX5(1−90)·RFXAP(135−272)	2:1	18910	35.0	32.9 ± 0.8
RFX5(1−90)·RFXAP(135−272)·RFXB	2:1:1	42860	63.4	59.3 ± 0.8
RFX5(1−170)·RFXAP	2:1	52260	66.6	62.2 ± 2.0
RFX5(1−170)·RFXAP·RFXB	2:1:1	76210	95.0	94.7 ± 3.5
RFX5(1−330)·RFXAP peak 1	4:1	115060	173.3	168.7 ± 8.7
RFX5(1−330)·RFXAP peak 2	2:1	63260	100.9	95.2 ± 1.4
RFX5(1−330)·RFXAP·RFXB peak 1	4:1:1	139010	201.7	227.2 ± 7.4
RFX5(1−330)·RFXAP·RFXB peak 2	2:1:1	87210	129.3	125.9 ± 4.4
RFX5(1−90,L66A)·RFXAP	1:1	15930	38.1	37.9 ± 2.1
RFX5(1−90,L66A)·RFXAP·RFXB	1:1:1	39880	66.5	54.1 ± 0.5
RFX5(1−170,L66A)·RFXAP	2:1	52260	66.5	56.2 ± 2.2
RFX5(1−170,L66A)·RFXAP·RFXB	2:1:1	76210	94.9	95.7 ± 9.2
RFX5(1−330,L66A)·RFXAP	2:1	63260	100.8	77.2 ± 0.7
RFX5(1−330,L66A)·RFXAP·RFXB	2:1:1	87210	129.2	122.8 ± 1.2

[a] The theoretical extinction coefficient was calculated using the equation proposed by Pace et al. (*35*). [b] The solution mass and error were calculated from the results of at least three independent SEC-SLS experiments. [c] The theoretical mass was calculated on the basis of the number of polypeptide chains and the theoretical mass of a monomer. The theoretical mass of a monomer was calculated using the amino acid sequence.

was separated from the complex during size exclusion. To determine the ratio of the two proteins in each complex, extinction coefficients that corresponded to different ratios of each protein were calculated. The ratio that gave the closest agreement between the theoretical molecular mass and the mass calculated by the light scattering measurements was selected (Table 3). To analyze complex formation between all three RFX proteins, the complexes formed between the RFX5 constructs and RFXAP in the previous experiments were concentrated to between 50 and 100 μM. The concentration was calculated on the basis of the extinction coefficients for each respective complex. For the RFX5(1−90) + RFXAP complex, the extinction coefficient for the 1:1 complex was used. For the RFXAP(1−170) + RFXAP and the RFX5(1−90) + RFXAP complexes, the extinction coefficient for the 2:1 complex was used. The RFX5 + RFXAP complex solutions were mixed in an equimolar amount with RFXB, and 200 μL was loaded onto the size exclusion column. The ratio of the three proteins in the complex was calculated as described for the complexes containing two proteins (Table 3).

Cross-Linking Studies of the RFX Proteins and Protein Complexes. Chemical cross-linking of the RFX proteins was performed using 1-ethyl-3-[3-(diethylamino)propyl]carbodiimide hydrochloride (EDC). The efficiency of the cross-linking was improved by the addition of *N*-hydroxysuccinimide (NHS). A stock solution of 100 mM EDC and 100 mM NHS in 20 mM phosphate, pH 7.0 and 150 mM NaCl was prepared prior to each cross-linking experiment. For analysis of the cross-linking reaction by SDS−PAGE 16 μL of the 100 mM EDC/NHS solution was added to a 64 μL solution containing the individual RFX proteins. Aliquots (16 μL) were removed after 0, 20, 40, and 60 min and added to 4 μL of SDS loading buffer. The SDS loading buffer contained 2.5 M 2-mercaptoethanol and 250 mM tris(hydroxymethyl)amine, both of which inhibit the cross-linking reaction. Samples (20 μL) were loaded onto SDS−PAGE gels and were stained either with Coomassie blue or silver stain (Bio-Rad), depending on the concentration of protein used during cross-linking (Figure 2). For each protein, a variety of concentrations were analyzed to determine the effect of protein concentration on oligomerization. The lower limit on protein concentration used depended on the efficiency of staining of the silver stain. All proteins were tested down to a concentration of 2.5 μM or less. The cross-linking studies of the RFX complexes were performed in an identical manner to the individual proteins. The complexes used for the cross-linking experiments were obtained from the SEC-SLS experiments. For analysis of the cross-linking reaction of RFX5(1−90) + RFXAP and RFX5(1−170) + RFXAP by mass spectrometry, 800 μL of the 100 mM protein complex was mixed with 200 μL of 100 mM EDC/NHS cross-linking solution. After 40 min the cross-linking reaction was stopped by addition of 100 μL of 1 M tris(hydroxymethyl)amine at pH 7.0. The solution was dialyzed into 10 mM ammonium acetate, pH 7.0, concentrated to 50 μL, and stored at −20 °C until use. Mass spectrometry data were collected on a Bruker Autoflex MALDI-TOF mass spectrometer (Center for Structural Biochemistry in the Chemistry Department at UMBC).

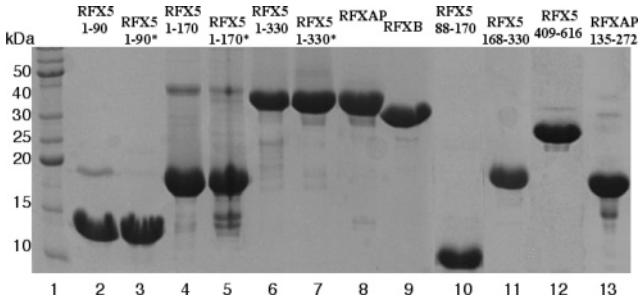

FIGURE 2: Coomassie-stained SDS−PAGE gel of the purified RFX proteins. The asterisk represents proteins containing the L66A mutation. Lanes: 1, molecular mass markers; 2, RFX5(1−90); 3, RFX5(1−90,L66A); 4, RFX5(1−170); 5, RFX5(1−170,L66A); 6, RFX5(1−330); 7, RFX5(1−330,L66A); 8, RFXAP; 9, RFXB; 10, RFX5(88−170); 11, RFX5(168−330); 12, RFX5(409−616); 13, RFXAP(135−272).

Analytical Ultracentrifugation Studies. Equilibrium sedimentation analytical ultracentrifugation was performed on RFX5(1−90), RFX5(1−90,L66A), RFX5(1−170), RFX5(1−170,L66A), and the RFX5(1−90) + RFXAP + RFXB complex using a Beckman XL-I Optima system (Beckman

Coulter). The proteins were prepared in 10 mM sodium phosphate buffer at pH 7.0 containing 150 mM NaCl and 1 mM DTT. Equilibrium sedimentation experiments were performed at 20 °C using rotor speeds between 15000 and 25000 rpm for 80 μM RFX5(1−90), 25 μM RFX5(1−170), 40 μM RFX5(1−170,L66A), and 5 μM RFX5(1−90) + RFXAP + RFXB complex. Rotor speeds between 20000 and 30000 rpm were used for 145 μM RFX5(1−90,L66A). Radial scans at 280 nm were collected between 6.3 and 7.3 cm as the average of five measurements, with a step size of 0.001 cm. The samples were allowed 19 h to achieve sedimentation equilibrium, which was confirmed by superimposing the scans collected after 18 and 19 h. Partial specific volumes and buffer densities were calculated in SEDNTERP (*36*) and the resultant data were processed using NONLIN (*37*).

RESULTS

Production of the RFX Proteins. All of the RFX proteins and protein fragments that were expressed and purified are summarized in Figure 1A. Full-length RFXB and RFXAP were expressed in *E. coli* bacterial cells and purified to homogeneity. Full-length RFX5 and RFX5 constructs containing the proline-rich region gave very low levels of expression in bacterial cells and did not produce sufficient yields for biophysical studies. RFX5(1−330) was the longest fragment that gave milligram quantities of protein with high purity. In addition to RFX5(1−330), several other constructs of RFX5 were expressed and purified in order to analyze their effects on oligomerization and complex formation. RFXB and the RFX5 constructs were expressed with an affinity tag containing a polyhistidine sequence and a TEV protease cleavage site. These proteins were purified using a nickel-charged HisTrap affinity column, ion exchange, and size exclusion chromatography. The affinity tag was removed during purification by the addition of TEV protease.

Full-length RFXAP could not be expressed alone in bacterial cells. Addition of a TEV protease cleavable N-terminal affinity tag, containing the 50 amino acid chitin binding domain (CBD), resulted in significant overexpression of RFXAP. Upon lysis of cells containing expressed RFXAP, RFXAP was immediately subjected to proteolysis from the C-terminal end, despite the presence of protease inhibitors. When RFXAP was lysed in the presence of RFX5(1−90), the proteolysis was prevented. This supports observations that RFX5 interacts with the C-terminal region of RFXAP. RFXAP was therefore expressed with an affinity tag containing the CBD but no polyhistidine sequence. The cells containing RFXAP were lysed with RFX5(1−90), which contained a polyhistidine sequence. The two proteins coeluted from a nickel-charged HisTrap column as a stable complex. To isolate RFXAP from RFX5(1−90), a second nickel column run was performed under denaturing conditions. RFX5(1−90) bound to the nickel column whereas RFXAP was located in the flow through. RFXAP was renatured by slowly removing the urea used to denature the proteins. Renatured RFXAP was shown to form a complex with RFX5 in an identical manner to protein that was purified by a nondenaturing method, confirming that RFXAP was folded correctly. The affinity tag was removed by addition of TEV protease, and RFXAP was further purified by size exclusion chromatography. Purification of RFXAP by this method significantly reduced the previously observed proteolysis and allowed full-length RFXAP to be purified.

Oligomeric State of the RFX Proteins. The oligomeric state of the RFX proteins was identified using size exclusion chromatography (SEC) with static light scattering (SLS). Static light scattering differs from dynamic light scattering, which is commonly used to analyze the behavior of proteins in solution, by providing a direct measure of a protein's mass in solution (*38*). The intensity of light scattered by a homogeneous sample of protein is directly proportional to the mass and concentration of the protein. The concentration can be determined by the Beer−Lambert law through measuring the absorbance of the sample at 280 nm and using the extinction coefficient of the protein at that wavelength. Measurement of the intensity of light scattered by a protein sample can therefore provide a direct method to calculate the solution mass and has been shown to be accurate to within 5−10% of the protein's actual mass (*38*). Comparing the solution mass with the theoretical mass of the protein monomer, which is calculated from its amino acid sequence, allows the oligomeric state to be identified. Coupling a size exclusion column with the light scattering detector allows separation of different oligomeric species that may be present. A Superdex 200 HR 10/30 column was used for all of the RFX proteins except RFX5(1−330). For RFX5(1−330), a Superdex 200 HR 10/30 column and a Superose 6 HR 10/30 column were coupled in series. The light scattering signal was measured by a miniDAWN Tristar light scattering detector. Table 2 summarizes the results of the SEC-SLS experiments for the RFX proteins.

RFXB and RFXAP both eluted as single species from the Superdex 200 column with SLS calculated masses essentially identical to the monomer mass of each protein (Table 2). The oligomerization domain of RFX5, residues 1−90, eluted as a single species (Figure 3A) with a SLS calculated mass of 33.3 ± 0.9 kDa. This value lies between the mass of a trimer (28.9 kDa) and a tetramer (38.6 kDa), suggesting that RFX5(1−90) forms a tetramer in solution but partially dissociates during size exclusion. The RFX5-RFX domain, residues 88−170, also eluted as a single species, and the mass calculated from SLS was close to that predicted for a monomer. Coupling the oligomerization domain to the RFX5-RFX domain, residues 1−170, resulted in two species eluting from the size exclusion column (Figure 3B). The SLS calculated mass of the major species was 72.7 ± 1.0 kDa, which is in good agreement with the theoretical mass of a tetramer (76.3 kDa). The second minor species had an SLS calculated mass of 50.9 ± 2.1 kDa, which lies between the mass of a dimer (38.1 kDa) and a trimer (57.2 kDa). This likely reflects an inability to resolve the different oligomeric species. Repeating size exclusion at different concentrations of RFX5(1−170) showed that the tetrameric form of RFX5-(1−170) was in excess at 20 μM, but as the concentration was reduced, the smaller oligomeric form was the dominant species (Figure 3C). The helical domain, residues 168−330, eluted as a single species with a SLS calculated mass of 31.8 ± 0.5 kDa, which is in close agreement to the theoretical mass of a dimer (35.2 kDa). Coupling the oligomerization domain, the RFX5-RFX domain, and the helical domain, residues 1−330, resulted in a mixture of two major species eluting from the Superose 6−Superdex 200 columns (Figure

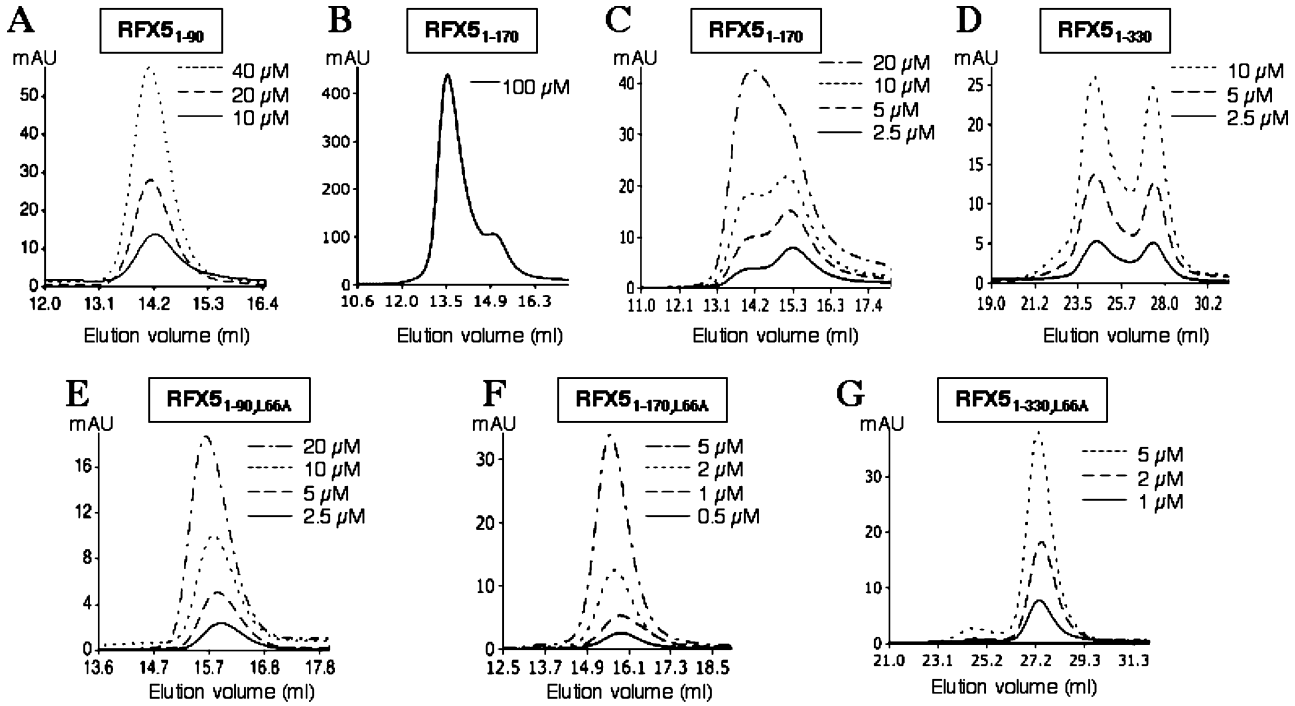

FIGURE 3: Size exclusion of the RFX5 constructs at different concentrations. The concentrations given are for the monomer. Panels: (A) RFX5(1−90), (B) RFX5(1−170) at high concentration, (C) RFX5(1−170) at low concentration, (D) RFX5(1−330), (E) RFX5(1−90,-L66A), (F) RFX5(1−170,L66A), and (G) RFX5(1−330,L66A).

3D). The higher molecular mass species gave a SLS calculated mass of 132.3 ± 7 kDa, which agrees with the theoretical mass of a tetramer (144.9 kDa). The second species gave a SLS calculated mass of 81.1 ± 0.3 kDa, which is similar to the theoretical mass of a dimer (72.4 kDa). Comparison of the elution profiles for different concentrations of RFX5(1−330) revealed that the tetrameric species was in slight excess at 10 μM, but the two species formed in equivalent amounts at 2.5 μM. This suggests that at lower concentration the dimeric form of RFX5(1−330) will likely predominate. The activation domain, residues 409−616, eluted from the Superdex 200 column as a single species with an SLS calculated mass of 24.2 ± 0.5 kDa, which is in close agreement with the theoretical mass of a monomer (22.2 kDa).

Cross-Linking Analysis of the Individual RFX Proteins. Chemical cross-linking was used to provide independent evidence of the oligomeric state of the RFX proteins. Cross-linking was performed with EDC, a zero-length cross-linking agent that promotes formation of a peptide bond between carboxyl groups and primary amines. The reaction was performed in the presence of *N*-hydroxysuccinimide to improve the efficiency of peptide bond formation. Samples were taken out over a period of an hour, and the cross-linking was quenched by the addition of excess tris(hydroxymethyl)-amine. The cross-linking was then analyzed as a function of time using SDS−PAGE.

RFXB, which was shown to be a monomer by SLS, was rapidly cross-linked to an aggregated species that was trapped in the loading well of the gel (Figure 4A). The aggregated species was still evident when the EDC/NHS reaction was performed at 10 μM RFXB (data not shown). This suggests that RFXB has a weak propensity to self-associate. RFXAP remained unchanged on exposure to EDC/NHS (data not shown), in agreement with the SLS results that RFXAP is a

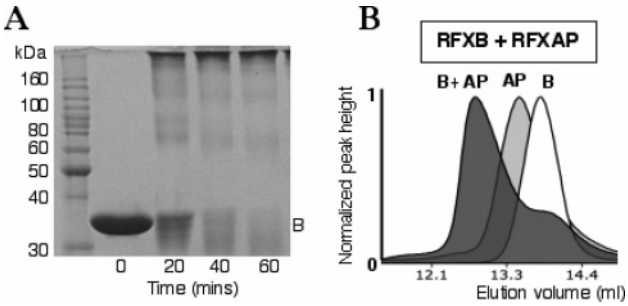

FIGURE 4: Analysis of RFXB and its interaction with RFXAP. (A) Cross-linking of RFXB. (B) Size exclusion of RFXB (white peak), RFXAP (light gray peak), and RFXB + RFXAP (dark gray peak). The gels are stained with Coomassie blue.

monomer. Cross-linking of RFX5(1−90) gave four bands on the SDS−PAGE gel, which is indicative of the formation of a tetramer (Figure 5A). The presence of the second and third bands on the gel does not imply the presence of a dimer or trimer but simply intermediates formed during cross-linking. SEC-SLS was also performed on the cross-linked RFX5(1−90) and revealed that it had a mass of 38.4 ± 0.4 kDa, which is in excellent agreement with the mass of a tetramer (38.6 kDa) (Table 2). This supports our hypothesis that RFX5(1−90) forms a tetramer but partially dissociates during SEC. The cross-linking of RFX5(1−90) prevents this dissociation from occurring. Cross-linking of RFX5(1−170) also suggested the formation of a tetramer, which agreed with the SEC-SLS studies (Figure 5B). The EDC/NHS reaction for RFX5(1−170) was not as efficient as it was for RFX5(1−90), which likely reflects the dissociation of RFX5-(1−170) to lower oligomeric states that was observed during SEC. Cross-linking of RFX5(168−330), the helical domain, showed two bands on the gel, which supports the SLS studies that the helical domain forms dimers (Figure 5C). The EDC/

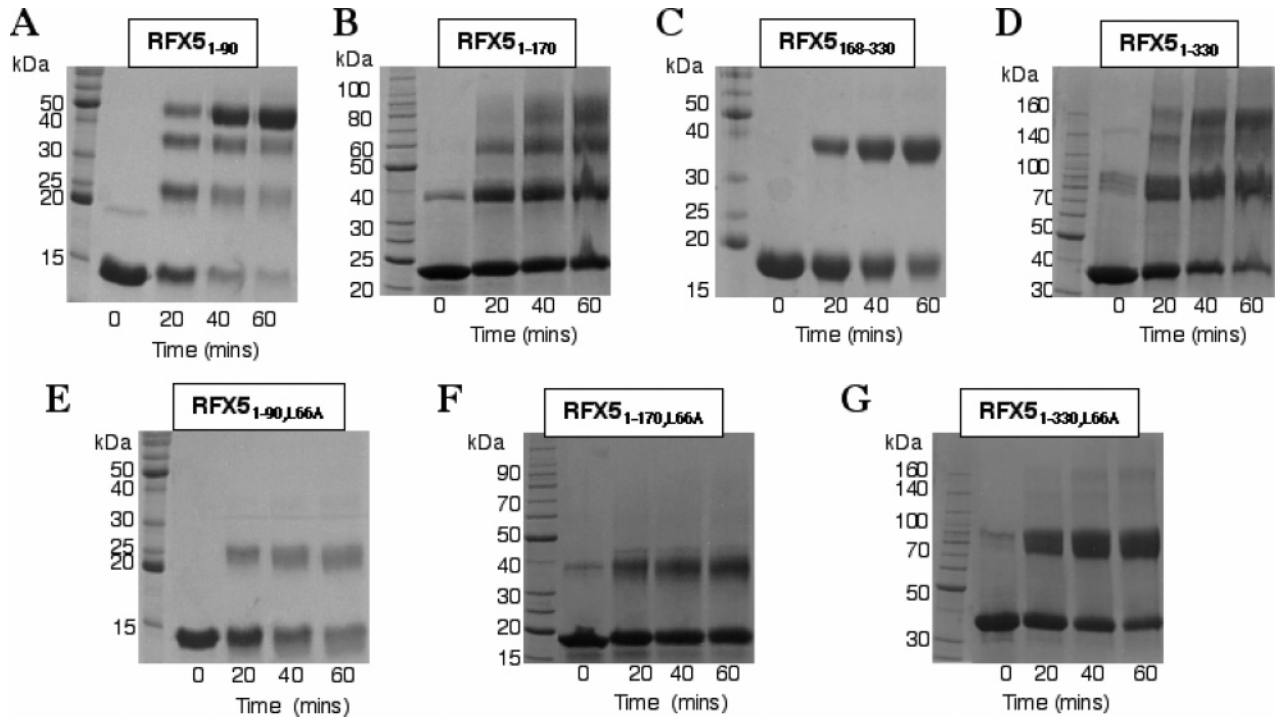

FIGURE 5: EDC cross-linking of RFX5 constructs: (A) 100 μM RFX5(1−90), (B) 50 μM RFX5(1−170), (C) 100 μM RFX5(168−330), (D) 25 μM RFX5(1−330), (E) 100 μM RFX5(1−90,L66A), (F) 50 μM RFX5(1−170,L66A), and (G) 25 μM RFX5(1−330,L66A). The gels are stained with Coomassie blue.

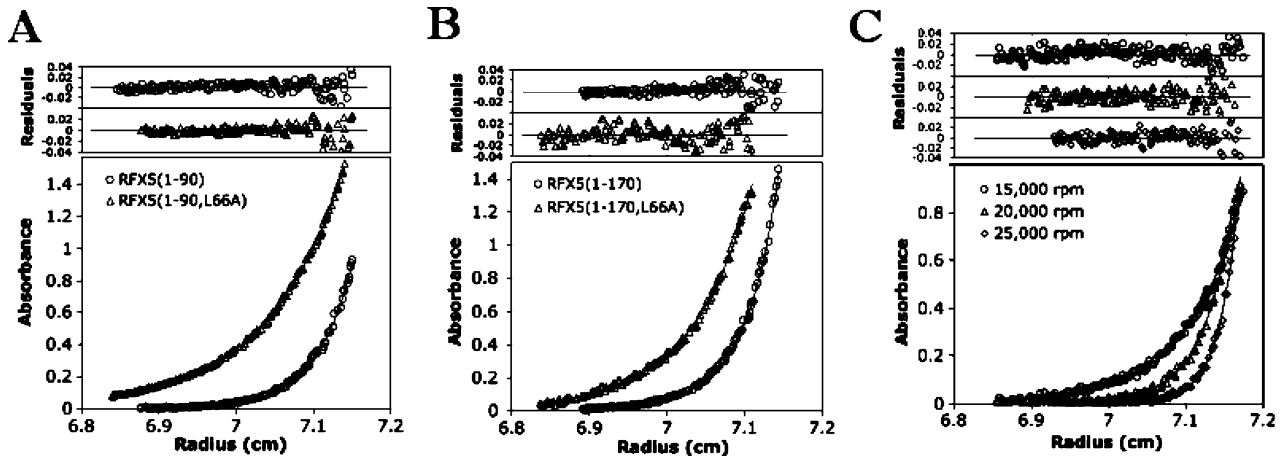

FIGURE 6: Sedimentation equilibrium data for RFX5. The absorbance versus radius profile is shown in the lower panel with the curved line representing the fit for the model applied to each protein (discussed in the text). The residuals of the fit are shown in the upper panels. (A) Representative data for RFX5(1−90) (circles), which was fit as a single species, and RFX5(1−90,L66A) (triangles), which was fit to a monomer−dimer equilibrium. (B) Representative data for RFX5(1−170) (circles), which was fit to a dimer−tetramer equilibrium, and RFX5(1−170,L66A) (triangles), which was fit to a monomer−dimer equilibrium. (C) Data for the RFX5(1−90)·RFXAP·RFXB complex, which was fit as a single species.

NHS reaction of RFX5(1−330) showed four bands, which is indicative of four cross-linked monomers (Figure 5D). This agrees with the SEC-SLS experiments that showed RFX5-(1−330) exists in an equilibrium between a dimeric and a tetrameric species. Exposing RFX5(88−170) and RFX5-(409−616) to EDC/NHS did not result in cross-linking (data not shown), which supports the SLS experiments that they form monomers in solution. The same pattern of cross-linking was observed for RFX5(1−90), RFX5(1−170), RFX5(168−330), and RFX5(1−330) for concentrations in the range of 1−5 μM (data not shown).

RFX5(1−170) Exists in a Dimer−Tetramer Equilibrium. The SEC-SLS studies of RFX5(1−90) and, in particular, RFX5(1−170) suggested that they exist in an equilibrium between a tetramer and a lower order oligomeric species. To investigate this further, we performed sedimentation equilibrium (SE) analytical ultracentrifugation experiments on RFX5(1−90) and RFX5(1−170) at three centrifugal speeds (Figure 6A,B). The SE data for RFX5(1−90) was best fit as a single species with an estimated mass of 39.2 ± 1.5 kDa, which is in excellent agreement with the predicted mass of a tetramer (38.8 kDa). The SE data for RFX5(1−170) gave the best fit for a dimer−tetramer equilibrium with a dissociation constant (K_d) for the tetramer of 1.7 ± 0.7 μM. These results suggest that the presence of domains C-terminal to the oligomerization domain destabilizes the formation of a dimer of dimers. This is potentially due to steric hindrance between the RFX5-RFX domains, which are

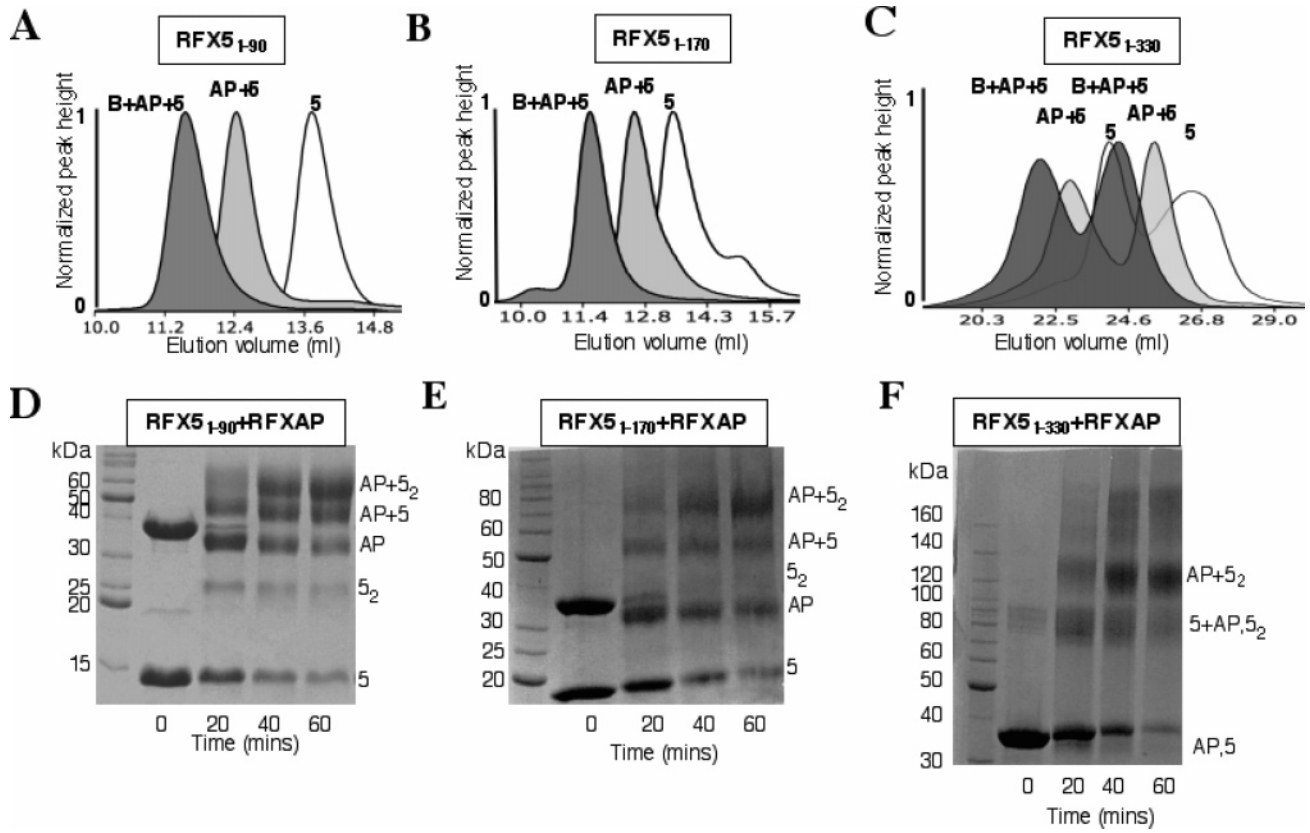

FIGURE 7: Size exclusion and cross-linking of the RFX5 complexes. (A) Size exclusion of RFX5(1−90), RFX5(1−90) + RFXAP, and RFX5(1−90) + RFXAP + RFXB. (B) Size exclusion of RFX5(1−170), RFX5(1−170) + RFXAP, and RFX5(1−170) + RFXAP + RFXB. (C) Size exclusion of RFX5(1−330), RFX5(1−330) + RFXAP, and RFX5(1−330) + RFXAP + RFXB. (D) EDC cross-linking of 25 μM RFX5(1−90) + RFXAP. (E) EDC cross-linking of 25 μM RFX5(1−170) + RFXAP. (F) EDC cross-linking of 12.5 μM RFX5-(1−330) + RFXAP. The size exclusion peaks for the RFX5, RFX5 + RFXAP, and RFX5 + RFXAP + RFXB are shown in white, light gray, and dark gray, respectively. The identities of the cross-linked species are shown on the right of the SDS−PAGE gels. The gels are stained with Coomassie blue.

likely located in close proximity to each other as a result of the tetramerization of the oligomerization domains.

RFXB Forms a Weak Complex with RFXAP. SEC-SLS and cross-linking experiments were used to determine which RFX proteins formed complexes and what the stoichiometry of the resultant complexes was. The results of the SEC-SLS experiments are given in Table 3. Size exclusion of RFXB and RFXAP showed they formed a complex, but the interaction was weak and the complex partially dissociated during the size exclusion (Figure 4B). To confirm that the second peak was not due to an excess of RFXB and RFXAP, the fractions for the complex were concentrated and passed over the Superdex column a second and third time. Identical elution profiles were obtained each time. The ratio of RFXB·RFXAP that gave a SLS-calculated mass closest to the theoretical mass was 1:1, although the two mass estimates differed significantly (theoretical mass was 56.8 kDa, the SLS calculated mass was 41.7 ± 3.2 kDa). This supports the observation that the complex partially dissociates during size exclusion, resulting in a mixture of complexed and free RFXB and RFXAP. The rapid cross-linking of RFXB with itself made the analysis of the EDC/NHS cross-linking experiments of RFXB + RFXAP and other complexes containing RFXB difficult to interpret.

RFX5(1−90) Is Sufficient To Form a Complex with RFXAP and RFXB. RFX5(1−90) and RFXB were not observed to interact during size exclusion and eluted at volumes identical to the proteins alone (data not shown). In contrast, RFX5(1−90) and RFXAP eluted together as a complex (Figure 7A), which confirms that the oligomerization domain of RFX5 is sufficient to form a complex with RFXAP. The SLS calculated mass for a 1:1 complex was 40.2 ± 0.3 kDa, which agrees with the theoretical mass of 38.1 kDa. In contrast to the interaction between RFXAP and RFXB, the RFX5(1−90) + RFXAP complex bound tightly to RFXB, suggesting that the affinity of RFXB for RFXAP is increased when RFXAP is bound to RFX5(1−90). The SLS calculated mass for a 1:1:1 complex was 66.3 ± 2.3 kDa, which gave excellent agreement with the theoretical mass of 66.5 kDa.

Chemical cross-linking of RFX5(1−90) + RFXAP gave five bands on an SDS−PAGE gel (Figure 7D). The band at 13 kDa likely corresponds to a monomer of RFX5(1−90). The second band, at approximately 26 kDa, has the same mobility as two cross-linked RFX5(1−90) monomers. The band at 36 kDa likely corresponds to RFXAP, which has previously been observed to run anomalously on SDS−PAGE gels relative to its actual mass (*20*). The shift in the RFXAP band to 32 kDa during cross-linking of the complex is consistent with intramolecular cross-linking of RFXAP, which was observed when cross-linking was performed with RFXAP alone (data not shown). Relative to the mass observed for the individual proteins on the gel, the band that occurs at approximately 47 kDa likely corresponds to cross-linking between a monomer of RFXAP and a monomer of RFX5(1−90). Similarly, the band at 59 kDa is likely to

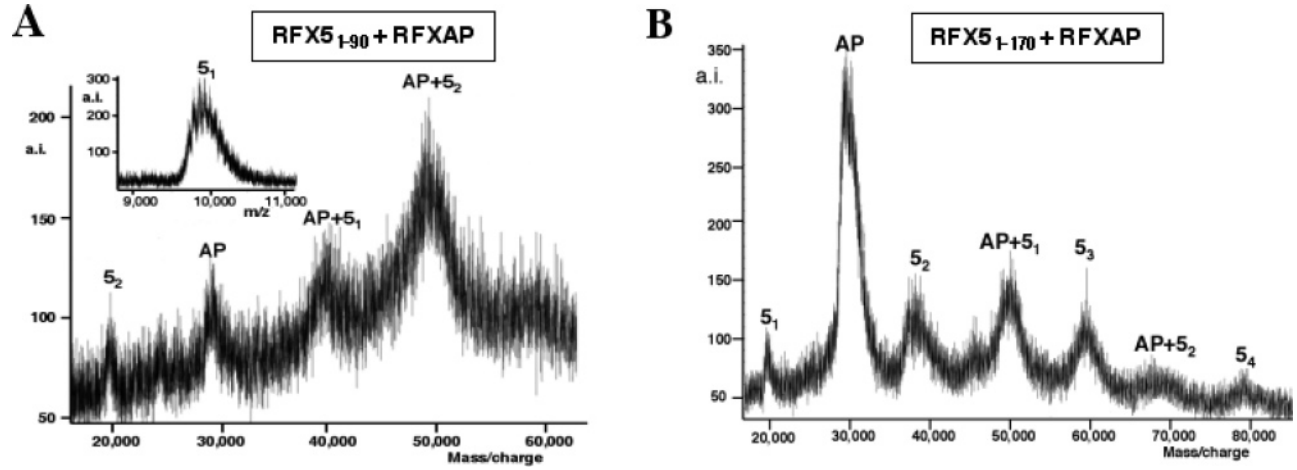

FIGURE 8: MALDI-TOF mass spectrometry analysis of cross-linked RFX5 + RFXAP complexes. (A) Mass spectrum of cross-linked RFX5(1−90) + RFXAP. (B) Mass spectrum of cross-linked RFX5(1−170) + RFXAP.

represent to cross-linking between two monomers of RFX5-(1−90) and a monomer of RFXAP. The cross-linking therefore suggests that a dimer of RFX5(1−90) interacts with a monomer of RFXAP.

In addition to SDS−PAGE, the cross-linking of the complex was analyzed by MALDI-TOF mass spectrometry (Figure 8A). In the resulting spectrum, each cross-linked species is represented by a cluster of peaks. The set of peaks in each cluster corresponds to the same overall cross-linked species, but their mass differs as a result of a different number of intramolecular and intermolecular cross-linked amino acids present. The spectrum for RFX5(1−90) + RFXAP shows five clusters, which are centered at 9, 20, 29, 41, and 50 kDa. Relative to the mass of the individual proteins, each peak could be assigned to a cross-linked species observed in the SDS−PAGE gel (Figure 8A), which supports the prediction of a 2:1 complex.

Chemical cross-linking experiments of the RFX5(1−90) + RFXAP + RFXB complex were not possible due to the extensive cross-linking of RFXB. We therefore performed a sedimentation equilibrium experiment on the complex using three centrifugal speeds (Figure 6C). The complex gave an excellent fit as a single species with a mass of 72.4 ± 3.3 kDa, which is in agreement with the predicted mass for a 2:1:1 stoichiometry of RFX5·RFXAP·RFXB (76.1 kDa).

The 2:1 ratio of RFX5·RFXAP obtained from cross-linking and the 2:1:1 ratio obtained for RFX5·RFXAP·RFXB from sedimentation equilibrium experiments are in contrast to the 1:1 and 1:1:1 ratios observed for the same complexes by SLS. Intriguingly, SEC-SLS experiments of the complex formed between RFX5(1−90) and a version of RFXAP that still had the CBD affinity tag attached gave a SLS calculated mass that corresponded to a 2:1 ratio of RFX5(1−90)·RFXAP (data not shown). This suggests that the N-terminal region of RFXAP may be able to affect the oligomeric state of RFX5(1−90) within the complex. To investigate the effect of the N-terminal end of RFXAP further, we expressed and purified RFXAP(135−272), which has previously been shown to complement the activity of full-length RFXAP in vivo (*39*). Size exclusion showed that RFX5(1−90) formed a complex with RFXAP(135−272), and the RFX5(1−90) + RFXAP(135−272) complex bound to RFXB (data not shown). The SLS calculated mass for the RFX5(1−90) + RFXAP(135−272) complex was 32.9 ± 0.8 kDa for a 2:1 ratio, which is in good agreement with the theoretical mass of 35.0 kDa. The SLS calculated mass for the RFX5(1−90) + RFXAP(135−272) + RFXB complex gave a SLS calculated mass of 59.3 ± 0.8 kDa for a 2:1:1 ratio, which is in close agreement with the theoretical mass of 63.4 kDa. These results support our hypothesis that the N-terminal region of RFXAP can modulate the oligomeric state of RFX5(1−90).

RFX5(1−170) Interacts with RFXAP and RFXB in a 2:1:1 Complex Ratio. Size exclusion showed that RFX5(1−170) eluted as a complex with RFXAP and that RFXB bound to the RFX5(1−170) + RFXAP complex (Figure 7B). The SLS calculated mass for a 2:1 ratio of the RFX5(1−170)·RFXAP complex was 62.2 ± 2.0 kDa, which agrees with the theoretical mass of 66.6 kDa. Similarly, the SLS calculated mass for a 2:1:1 ratio of RFX5(1−170)·RFXAP·RFXB was calculated to be 94.7 ± 3.5 kDa, which is in excellent agreement with the theoretical mass of 95.0 kDa. A second small peak was observed at higher molecular mass during size exclusion of both the RFX5(1−170) + RFXAP and the RFX5(1−70) + RFXAP + RFXB complexes. The concentrations of these species were too low to obtain an accurate reading of their mass by light scattering.

Chemical cross-linking analysis using SDS−PAGE supported the SLS calculated ratio of 2:1 for RFX5(1−170)·RFXAP (Figure 7E). Analysis of the cross-linking by mass spectrometry gave six peaks, which were located at 20, 30, 38, 50, and 68 kDa (Figure 8B). These peaks can be correlated with the five cross-linked species observed from SDS−PAGE and support the 2:1 ratio of RFX5·RFXAP. Two further cluster of peaks were observed, one at 58 kDa and another at 78 kDa. These peaks correspond to the mass of three and four cross-linked monomers of RFX5(1−170), respectively, and are likely due to excess free RFX5(1−170) that was not removed during purification.

RFX5(1−330) Interacts with RFXAP and RFXB in a 2:1:1 and 4:1:1 Ratio. Addition of RFXAP to RFX5(1−330) resulted in a shift in position of the peaks corresponding to both the dimer and the tetramer (Figure 7C). For the first peak, a 4:1 ratio of RFX5(1−330)·RFXAP gave a SLS calculated mass of 168.7 ± 8.7 kDa, which is in excellent agreement with the theoretical mass of 173.3 kDa. The second peak gave a SLS calculated mass of 95.2 ± 3.5 kDa for a 2:1 ratio of RFX5(1−330)·RFXAP, which is in close

agreement to the theoretical mass of 100.9 kDa. Interpretation of the cross-linking studies of the RFX5(1−330) + RFXAP complex was made difficult by the broadening of bands due to the length of the proteins involved and by the fact that RFXAP and RFX5(1−330) migrate at the same molecular mass on the SDS−PAGE gel. One major cross-linked species that was clearly evident corresponded to three cross-linked subunits, which would agree with the presence of the 2:1 complex of RFX5(1−330) + RFXAP (Figure 7F). The observation of further cross-linking would agree with the presence of the 4:1 complex as well as the 2:1 complex. Addition of RFXB to the RFX5(1−330) + RFXAP complex similarly resulted in a shift in both peaks to higher molecular mass (Figure 6C). The SLS calculated mass for the first peak was 227.2 ± 7.4 kDa for a 4:1:1 complex of RFX5(1−330)·RFXAP·RFXB, which is close to the theoretical mass of 201.7 kDa. The second peak gave a SLS calculated mass of 125.9 ± 4.4 kDa for a 2:1:1 complex, which is in excellent agreement with the theoretical mass of 129.3 kDa.

The RFX5(L66A) Point Mutation Disrupts Oligomerization of RFX5. The point mutant RFX5 (L66A) is predicted to affect oligomerization of the RFX complex and inhibit MHCII gene expression (*19*). To study the effect of RFX5-(L66A), the point mutation was introduced into RFX5-(1−90), RFX5(1−170), and RFX5(1−330) by site-directed mutagenesis, and the proteins were expressed and purified in a similar manner to the wild-type proteins. Size exclusion of RFX5(1−90,L66A) showed it eluted later than the RFX5-(1−90), suggesting its oligomeric state had been modified (Figure 3E). The SLS calculated mass for RFX5(1−90,-L66A) was 17.9 ± 1.1 kDa, which corresponds to the mass of a dimer (19.2 kDa) (Table 2). RFX5(1−170,L66A) gave one peak during size exclusion and eluted at the same volume as the second peak of RFX5(1−170) (Figure 3F). The SLS calculated mass for RFX5(1−170,L66A) was 33.5 ± 1.5 kDa, which corresponds to a dimer (38.2 kDa). RFX5-(1−330,L66A) eluted from the Superose 6−Superdex 200 columns as a single species with the same elution volume as the RFX5(1−330) dimer (Figure 3G). The SLS calculated mass for this peak was 73.8 ± 2.2 kDa, which is in excellent agreement with the theoretical mass of a dimer (72.3 kDa). A small peak was evident at the elution volume corresponding to the RFX5(1−330) tetramer, but its concentration was too low to measure the mass by SLS.

Cross-linking of RFX5(1−90,L66A), RFX5(1−170,-L66A), and RFX5(1−330,L66A) all showed two bands on the SDS−PAGE gel, which indicates they form dimers (panels E, F, and G of Figure 5, respectively). This agrees with the SEC-SLS studies of the same fragments. Formation of the dimeric forms was also evident in cross-linking experiments performed with concentrations between 1 and 5 μM protein (data not shown). The cross-linking and SEC-SLS experiments provide direct evidence that the L66A point mutant inhibits dimerization between two RFX5 dimers.

The deviation between the predicted mass and the SLS calculated mass of RFX5(1−90,L66A) and RFX5(1−170,-L66A) suggested that the dimer may dissociate to form an amount of monomer as well. To investigate this, we repeated the equilibrium sedimentation experiments using RFX5-(1−90,L66A) and RFX5(1−170,L66A) (Figure 6A,B). The SE data for RFX5(1−90,L66A) fit best to a monomer−dimer equilibrium with a K_d of 2.1 ± 1.1 μM for the dimer. The SE data for RFX5(1−170,L66A) gave the best fit for a monomer−dimer equilibrium with a K_d of 0.21 ± 0.13 μM for the dimer. These results suggest that both RFX5(1−90,-L66A) and RFX5(1−170,L66A) exist as dimers at micromolar concentration and that the RFX5(1−170,L66A) dimer is more stable than the RFX5(1−90,L66A) dimer.

The RFX5(L66A) Point Mutation Does Not Prevent Formation of the RFX Complex. To determine the effect of the point mutation on complex assembly, we tested the ability of RFX5(1−90,L66A), RFX5(1−170,L66A), and RFX5-(1−330,L66A) to interact with RFXAP and RFXB. SEC experiments showed that RFX5(1−90,L66A) and RFX5-(1−170,L66A) behaved in an identical manner to the wild-type proteins (panels A and B of Figure 9, respectively), and SLS studies showed they formed similar complexes (Table 3). RFX5(1−330,L66A) formed a stable complex with RFXAP similar to RFX5(1−330) but gave one major complex species that eluted at the same location as the 2:1 complex of RFX5(1−330)·RFXAP (Figure 9C). A ratio of 2:1 gave the closest agreement between the SLS calculated mass of 77.2 ± 0.7 kDa and the theoretical mass of 100.8 kDa. The cause of the difference in the two masses is unclear. Addition of RFXB to this complex resulted in the complex eluting at the same location as the 2:1:1 complex of RFX5-(1−330) + RFXAP + RFXB. The SLS calculated mass for a 2:1:1 ratio was 122.8 ± 1.2 kDa, which is in good agreement with the calculated mass of 129.2 kDa.

Cross-linking of the RFX5(1−90,L66A) + RFXAP and RFX5(1−170,L66A) + RFXAP complexes gave identical results to the wild-type complexes (Figure 9D,E). The RFX5-(1−330,L66A) + RFXAP complex gave similar results as the wild-type complex but did not show appreciable cross-linked species past the band corresponding to the 2:1 complex, in agreement with the inability of this complex to further oligomerize (Figures 9F). The results of the SEC-SLS and cross-linking provide direct evidence that the point mutation does not affect complex formation but does inhibit dimerization between an RFX complex and a second RFX5 dimer.

DISCUSSION

We have used static light scattering, chemical cross-linking, and analytical ultracentrifugation to characterize the oligomeric states of the individual proteins that make up the RFX complex and to determine the ratios of their subsequent complexes.

Oligomeric State of the RFX Proteins. We have shown that both RFXB and RFXAP form monomers in solution, which is in agreement with previous analytical ultracentrifugation experiments on insect cell expressed RFXB and RFXAP (*29*). The EDC/NHS cross-linking experiments also revealed that RFXB has a propensity to self-associate in solution, although this interaction is presumably weak as it is not observed during size exclusion. Whether the ability of RFXB to self-associate has a physiological role is yet to be determined.

Previous studies of RFX5 and the complexes it forms by analytical ultracentrifugation have been complicated by the formation of multiple oligomeric states (*29*). We have resolved and characterized the different oligomeric states that RFX5 adopts, and we have identified the regions of RFX5

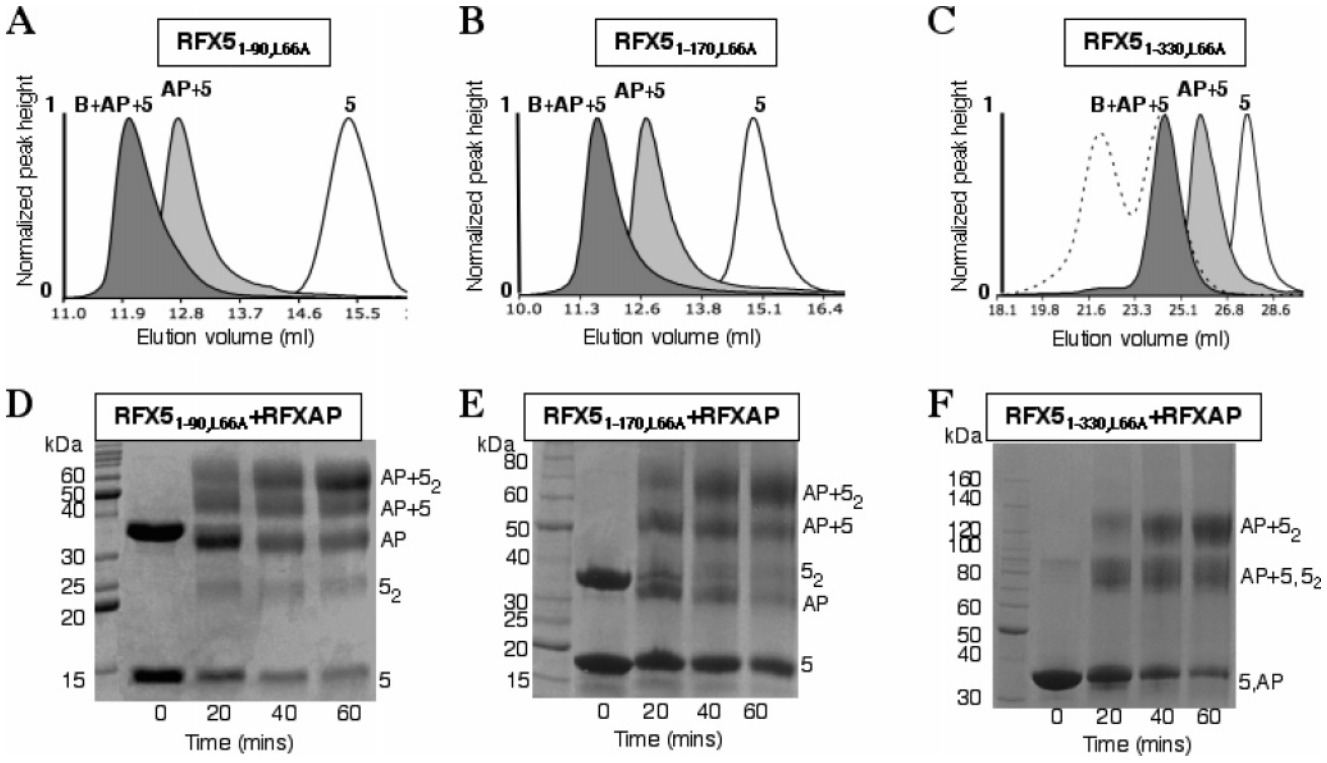

FIGURE 9: Size exclusion and cross-linking of RFX5(L66A) complexes. (A) Size exclusion of RFX5(1−90,L66A), RFX5(1−90,L66A) + RFXAP, and RFX5(1−90,L66A) + RFXAP + RFXB. (B) Size exclusion of RFX5(1−170,L66A), RFX5(1−170,L66A) + RFXAP, and RFX5(1−170,L66A) + RFXAP + RFXB. (C) Size exclusion of RFX5(1−330,L66A), RFX5(1−330,L66A) + RFXAP, and RFX5-(1−330,L66A) + RFXAP + RFXB. The dashed line represents the wild-type RFX5(1−330) + RFXAP + RFXB complex for reference. (D) Cross-linking of 25 μM RFX5(1−90,L66A) + RFXAP. (E) Cross-linking of 25 μM RFX5(1−170,L66A) + RFXAP. (F) Cross-linking of 12.5 μM RFX5(1−330,L66A) + RFXAP. The size exclusion peaks for the RFX5, RFX5 + RFXAP, and RFX5 + RFXAP + RFXB are shown in white, light gray, and dark gray, respectively. The identities of the cross-linked species are shown on the right of the SDS−PAGE gels. The gels are stained with Coomassie blue.

that promote the oligomerization. RFX5 contains two dimerization domains, the oligomerization domain (residues 1−90) and the helical domain (residues 168−330). The constructs containing only the oligomerization domain, RFX(1−90) and RFX5(1−170), both formed tetrameric species, but as the concentration was lowered, RFX5(1−170) was observed to dissociate to a dimer. The K_d for the tetramer to dimer dissociation was determined by sedimentation equilibrium experiments to be 1.7 μM, suggesting that at physiological concentrations this domain is likely to form a dimer. The helical domain was shown to form dimers at all concentrations analyzed. Coupling the oligomerization domain and the helical domain together in the RFX5(1−330) construct gave a mixture of two species: a dimer and a tetramer. We therefore propose that at submicromolar concentrations RFX5(1−330) forms a dimer via the oligomerization domain and the helical domain, and we propose that RFX5(1−330) has the propensity to form a dimer of dimers through contacts made between the oligomerization domains from two RFX5 dimers (Figure 10A). Being unable to analyze constructs containing the proline-rich region, we cannot definitively state what effect this region will have on the oligomeric state of RFX5(1−330). However, the proline-rich region is comprised primarily of Pro (27%), Leu (15%), Ala (13%), and Gly (10%), and this amino acid composition strongly suggests that the region is unstructured. Together with the observation that RFX5(409−616) forms a monomer, this implies that the region between 330 and 616 is also monomeric and is unlikely to contribute to further oligomerization of RFX5. We therefore propose that RFX5-(1−330) represents a good model for full-length RFX5.

Interactions between the RFX Proteins. Previous studies have proposed that both the oligomerization domain and the helical domain of RFX5 contribute to the interaction with RFXAP and RFXB (*20*). We did not observe any interaction between the helical domain of RFX5 with either RFXAP, RFXB, or RFXAP + RFXB (data not shown). In contrast, the RFX5 oligomerization domain formed a stable complex with RFXAP in the absence or presence of RFXB. The interaction between RFX5 and RFXB in the literature is inconclusive as various studies suggested that they do interact (*19*, *20*, *25*) while others suggest they do not interact (*27*, *29*). We did not observe any interaction between the RFX5 constructs and RFXB. RFXAP and RFXB were observed to interact with each other, in agreement with several studies (*19*, *20*, *25*, *27*, *29*). This interaction is clearly weak as the complex readily dissociated during size exclusion at high micromolar concentration. In contrast, RFXB formed a very stable interaction with the RFX5 + RFXAP complexes. This implies that the RFX5 + RFXAP complexes form a higher affinity binding site for RFXB than RFXAP does on its own. This could occur as a result of an RFX5-induced conformational change in RFXAP that increases its affinity for RFXB, or RFX5 could contribute to the RFXAP−RFXB binding interface. These observations suggest that RFX5 and RFXAP are likely to form a complex prior to interacting with RFXB.

Anomalous Behavior of the RFX5(1−90) Complexes during SEC. The chemical cross-linking studies of the RFX5-

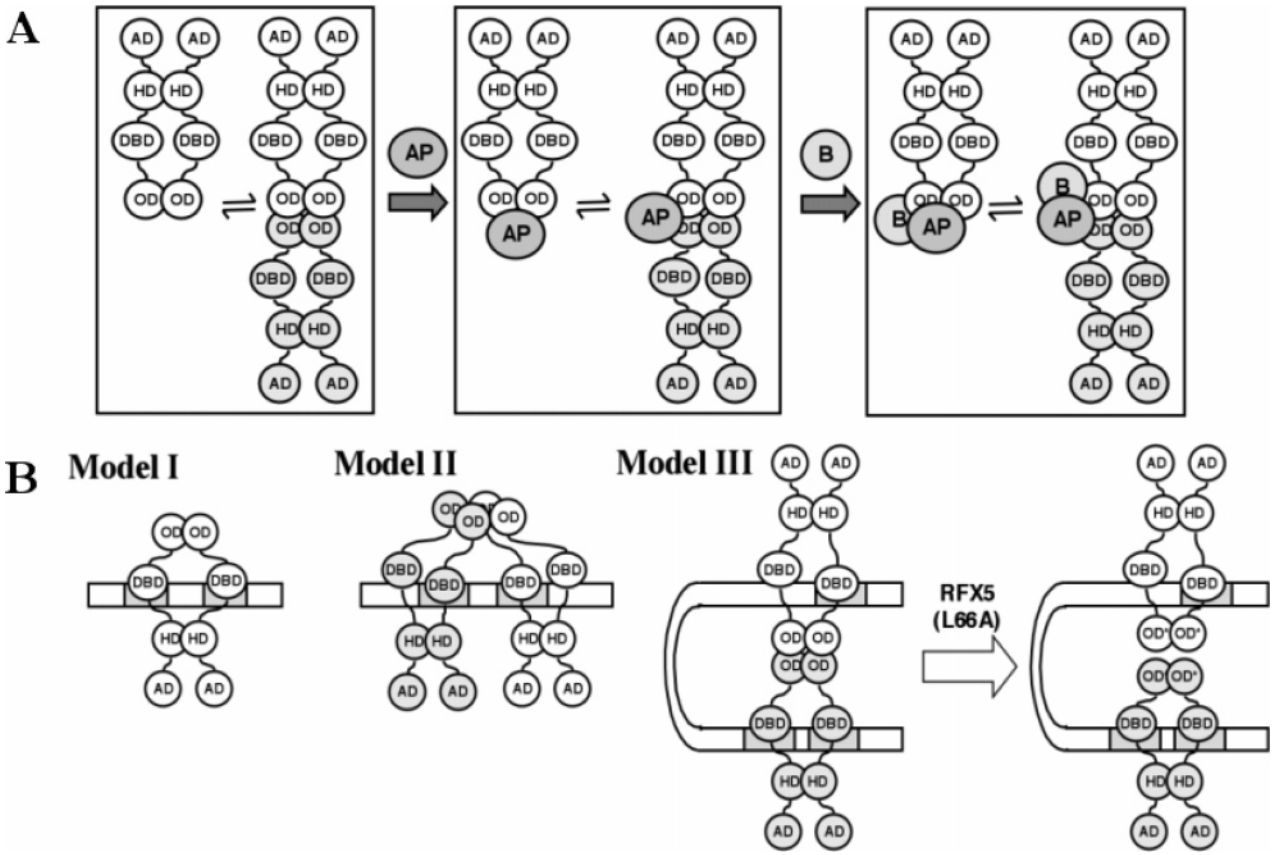

FIGURE 10: Models for the assembly of the RFX complex and how it interacts with the DNA. (A) Equilibrium of RFX5 and the complexes it forms. Acronyms are the same as described in Figure 1. RFXAP (AP) is shown in dark gray, and RFXB (B) is shown in light gray. (B) Potential models for the interaction between the RFX complex and DNA. RFXAP and RFXB are not shown for clarity. Model I: One RFX complex bound to both the S-box and the X1-box. Model II: Two RFX complexes bound to the S-box and X1-box. Model III: Two RFX complexes induce DNA looping through contacts to two X1-box sequences. The effect of the RFX5(L66A) point mutation is also shown for model III. OD* represents the mutated oligomerization domain.

(1−90) + RFXAP complex and the sedimentation equilibrium studies of the RFX5(1−90) + RFXAP + RFXB complex gave a 2:1 and a 2:1:1 ratio of RFX5·RFXAP and RFX5·RFXAP·RFXB, respectively. This is in agreement with the SEC-SLS studies of longer RFX5 fragments. In contrast, the SEC-SLS studies of the same complexes gave a 1:1 and a 1:1:1 ratio for the RFX5(1−90) + RFXAP and RFX5(1−90) + RFXAP + RFXB complexes, respectively. Formation of the 1:1 and 1:1:1 complexes during SEC appears to be dependent on an interaction between the N-terminus of RFXAP with RFX5(1−90) since modifying the N-terminal region of RFXAP, either by increasing its length with an affinity tag or deleting the N-terminal 134 amino acids, results in formation of 2:1 and 2:1:1 complexes. Taken into account all of the experimental observations made on the complexes formed by RFX5(1−90) and the other RFX5 constructs, we propose the following: We propose that a dimer of RFX5(1−90) interacts with a monomer of RFXAP and RFXB to form a 2:1:1 complex of RFX5·RFXAP·RFXB, but under certain circumstances the N-terminal region of RFXAP can modify the oligomeric state of RFX5(1−90).

Stoichiometries of the RFX Complexes. Both RFX5(1−90) and RFX5(1−170) form tetramers in solution. Addition of RFXAP results in the two proteins forming a 2:1 complex of RFX5·RFXAP. This suggests that RFXAP binds at or near the dimer−dimer interface and prevents formation of the tetramer. From these results we would predict that RFX5(1−330), which also forms a tetramer, would also interact with RFXAP in a 2:1 ratio. A complex containing a 2:1 ratio of RFX5(1−330)·RFXAP does occur, but a second species, comprising a 4:1 ratio, is also observed. The presence of a tetramer of RFX5(1−330) in the second complex suggests that RFXAP may bind to RFX5(1−330) in a different manner in the 4:1 complex compared to in the 2:1 complex. Alternatively, the dimer−dimer interface of the $RFX5(1-330)_4$·RFXAP complex may be different from that observed in the RFX5(1−330) tetramer. Although we could not identify the ratio of RFXB to RFXAP in the RFXB + RFXAP complex, RFXB is observed to bind to all of the RFX5 + RFXAP complexes in a 1:1 ratio with RFXAP, suggesting it interacts with RFXAP in a 1:1 ratio in the absence of RFX5. On the basis of these results, we propose the following model for RFX complex assembly (Figure 10A): A dimer of RFX5 interacts with a monomer of RFXAP through the RFX5 oligomerization domains. The interaction between RFX5 and RFXAP forms a high-affinity binding site for a monomer of RFXB. This binding site is likely to be comprised primarily of contacts from RFXAP. The entire RFX complex therefore has a RFX5·RFXAP·RFXB ratio of 2:1:1. The RFX complex can also interact with a further RFX5 dimer through intermolecular contacts made between the oligomerization domains of RFX5 to give a RFX5·RFXAP·RFXB ratio of 4:1:1.

DNA-Binding Models for the RFX Complex Binding to the MHCII Promoter. Previous studies of the MHCII

promoter have suggested that the RFX complex can bind either to both the S-box and the X1-box DNA sequences or only to the X1-box sequence (*19*, *31*). The evidence supporting the latter model was based on evidence that mutation of the S-box sequence has no effect on the amount of RFX complex bound to the MHCII promoter. We propose two potential models for RFX binding to the S-X1-box sequence that agree with the experimental data from both earlier models (Figure 10B). In the first model, the RFX complex contacts both the S-box sequence and the X1-box sequence through the two RFX5-RFX domains. Mutation of the S-box would result in loss of binding of one RFX5-RFX domain to DNA but would not affect the DNA binding of the second RFX5-RFX domain. Thus the amount of RFX bound to the MHCII promoter would be unchanged. In the second model, an RFX complex and a RFX5 dimer could bind cooperatively to the S-box and the X1-box through contacts made between the oligomerization domains. Mutation of the S-box would result in a loss of DNA binding of one RFX complex, but it would still remain associated with the other RFX complex through contacts made between the oligomerization domains.

Recently, the RFX complex has been proposed to induce DNA looping through contacts made to the proximal X1-box and to distal X1-box binding sites (*34*). We propose that this loop could be formed by the dimerization between an RFX complex bound to the proximal S−X1-box sequence with an RFX5 dimer bound to the distal X1-box sequence (Figure 10B). The formation of the loop would have a direct effect on the chromatin structure in the vicinity of the MHCII genes and, therefore, on their expression (*33*). The looping may also be necessary to bring together distal components required for regulating MHCII gene expression (*40*). The role of RFXB and RFXAP in DNA binding is not clear, although previous studies clearly show they have an important role in DNA binding of the RFX complex (*20*, *28*, *41*).

The importance of dimerization between RFX complexes in DNA binding and MHCII gene expression is supported by previous studies (*18*, *19*) and by our studies of the RFX5-(L66A) point mutation. Mutation of any of the leucine residues in the sequence 62-LYLYLQL-68 of RFX5 results in the loss of expression of the MHCII genes (*18*). This correlates with a loss in DNA binding of the RFX complex to the MHCII promoter (*19*). We directly show that the RFX5(L66A) point mutation does not inhibit assembly of the RFX complex but instead disrupts dimerization between two RFX5 dimers. The RFX5(L66A) mutation could therefore prevent cooperative interactions between an adjacently binding RFX complex and an RFX5 dimer, which may be essential for stability of the MHCII enhanceosome. Alternatively, RFX5(L66A) could prevent DNA looping, which may be necessary for chromatin remodeling at the MHCII genes or for bringing distal components together that are required for MHCII gene regulation (Figure 10B).

CONCLUSIONS

The studies presented here have characterized the assembly of the RFX complex and have connected the importance of dimerization between RFX complexes to MHCII gene expression. Future studies will address the stoichiometry of the interactions between the RFX complex and other components of the MHCII enhanceosome, as well as the details of the RFX−MHCII promoter interaction.

ACKNOWLEDGMENT

The authors thank Dr. Alexei Gapeev for assistance in collecting MALDI-TOF mass spectrometry data. We also thank Dr. Nicole LaRhonde-LeBlanc for assistance in collecting and processing the analytical ultracentrifugation data. Finally, we thank Drs. Veronika Szalai, Richard Karpel, and Graeme Conn for critical reading of the manuscript.

REFERENCES

1. Ting, J. P., and Zhu, X. S. (1999) Class II MHC genes: a model gene regulatory system with great biologic consequences, *Microbes Infect. 1*, 855−861.
2. Reith, W., and Mach, B. (2001) The bare lymphocyte syndrome and the regulation of MHC expression, *Annu. Rev. Immunol. 19*, 331−373.
3. Benoist, C., and Mathis, D. (1990) Regulation of major histocompatibility complex class-II genes: X, Y and other letters of the alphabet, *Annu. Rev. Immunol. 8*, 681−715.
4. Glimcher, L. H., and Kara, C. J. (1992) Sequences and factors: a guide to MHC class-II transcription, *Annu. Rev. Immunol. 10*, 13−49.
5. Carey, M. (1998) The enhanceosome and transcriptional synergy, *Cell 92*, 5−8.
6. Merika, M., and Thanos, D. (2001) Enhanceosomes, *Curr. Opin. Genet. Dev. 11*, 205−208.
7. Reith, W., Satola, S., Sanchez, C. H., Amaldi, I., Lisowska-Grospierre, B., Griscelli, C., Hadam, M. R., and Mach, B. (1988) Congenital immunodeficiency with a regulatory defect in MHC class II gene expression lacks a specific HLA-DR promoter binding protein, RF-X, *Cell 53*, 897−906.
8. Hasegawa, S. L., and Boss, J. M. (1991) Two B cell factors bind the HLA-DRA X box region and recognize different subsets of HLA class II promoters, *Nucleic Acids Res. 19*, 6269−6276.
9. Durand, B., Kobr, M., Reith, W., and Mach, B. (1994) Functional complementation of major histocompatibility complex class II regulatory mutants by the purified X-box-binding protein RFX, *Mol. Cell. Biol. 14*, 6839−6847.
10. Jabrane-Ferrat, N., Fontes, J. D., Boss, J. M., and Peterlin, B. M. (1996) Complex architecture of major histocompatibility complex class II promoters: reiterated motifs and conserved protein-protein interactions, *Mol. Cell. Biol. 16*, 4683−90.
11. Kara, C. J., and Glimcher, L. H. (1991) In vivo footprinting of MHC class II genes: bare promoters in the bare lymphocyte syndrome, *Science 252*, 709−712.
12. Durand, B., Sperisen, P., Emery, P., Barras, E., Zufferey, M., Mach, B., and Reith, W. (1997) RFXAP, a novel subunit of the RFX DNA binding complex is mutated in MHC class II deficiency, *EMBO J. 16*, 1045−1055.
13. Nagarajan, U. M., Louis-Plence, P., DeSandro, A., Nilsen, R., Bushey, A., and Boss, J. M. (1999) RFX-B is the gene responsible for the most common cause of the bare lymphocyte syndrome, an MHC class II immunodeficiency, *Immunity 10*, 153−162.
14. Masternak, K., Barras, E., Zufferey, M., Conrad, B., Corthals, G., Aebersold, R., Sanchez, J. C., Hochstrasser, D. F., Mach, B., and Reith, W. (1998) A gene encoding a novel RFX-associated transactivator is mutated in the majority of MHC class II deficiency patients, *Nat. Genet. 20*, 273−277.
15. Moreno, C. S., Rogers, E. M., Brown, J. A., and Boss, J. M. (1997) Regulatory factor X, a bare lymphocyte syndrome transcription factor, is a multimeric phosphoprotein complex, *J. Immunol. 158*, 5841−5848.
16. Steimle, V., Durand, B., Barras, E., Zufferey, M., Hadam, M. R., Mach, B., and Reith, W. (1995) A novel DNA-binding regulatory factor is mutated in primary MHC class II deficiency (bare lymphocyte syndrome), *Genes Dev. 9*, 1021−1032.
17. Emery, P., Durand, B., Mach, B., and Reith, W. (1996) RFX proteins, a novel family of DNA binding proteins conserved in the eukaryotic kingdom, *Nucleic Acids Res. 24*, 803−807.
18. Brickey, W. J., Wright, K. L., Zhu, X. S., and Ting, J. P. (1999) Analysis of the defect in IFN-gamma induction of MHC class II genes in G1B cells: identification of a novel and functionally

critical leucine-rich motif (62-LYLYLQL-68) in the regulatory factor X 5 transcription factor, *J. Immunol. 163*, 6622−6630.
19. Jabrane-Ferrat, N., Nekrep, N., Tosi, G., Esserman, L. J., and Peterlin, B. M. (2002) Major histocompatibility complex class II transcriptional platform: assembly of nuclear factor Y and regulatory factor X (RFX) on DNA requires RFX5 dimers, *Mol. Cell. Biol. 22*, 5616−5625.
20. DeSandro, A. M., Nagarajan, U. M., and Boss, J. M. (2000) Associations and interactions between bare lymphocyte syndrome factors, *Mol. Cell. Biol. 20*, 6587−6599.
21. Gajiwala, K. S., Chen, H., Cornille, F., Roques, B. P., Reith, W., Mach, B., and Burley, S. K. (2000) Structure of the winged-helix protein hRFX1 reveals a new mode of DNA binding, *Nature 403*, 916−921.
22. Villard, J., Peretti, M., Masternak, K., Barras, E., Caretti, G., Mantovani, R., and Reith, W. (2000) A functionally essential domain of RFX5 mediates activation of major histocompatibility complex class II promoters by promoting cooperative binding between RFX and NF-Y, *Mol. Cell. Biol. 20*, 3364−3376.
23. Nekrep, N., Geyer, M., Jabrane-Ferrat, N., and Peterlin, B. M. (2001) Analysis of ankyrin repeats reveals how a single point mutation in RFXANK results in bare lymphocyte syndrome, *Mol. Cell. Biol. 21*, 5566−5576.
24. Mosavi, L. K., Cammett, T. J., Desrosiers, D. C., and Peng, Z. Y. (2004) The ankyrin repeat as molecular architecture for protein recognition, *Protein Sci. 13*, 1435−1448.
25. Das, S., Lin, J. H., Papamatheakis, J., Sykulev, Y., and Tsichlis, P. N. (2002) Differential splicing generates Tvl-1/RFXANK isoforms with different functions, *J. Biol. Chem. 277*, 45172−45180.
26. Wiszniewski, W., Fondaneche, M. C., Louise-Plence, P., Prochnicka-Chalufour, A., Selz, F., Picard, C., Le Deist, F., Eliaou, J. F., Fischer, A., and Lisowska-Grospierre, B. (2003) Novel mutations in the RFXANK gene: RFX complex containing in-vitro-generated RFXANK mutant binds the promoter without transactivating MHC II, *Immunogenetics 54*, 747−755.
27. Nekrep, N., Jabrane-Ferrat, N., and Peterlin, B. M. (2000) Mutations in the bare lymphocyte syndrome define critical steps in the assembly of the regulatory factor X complex, *Mol. Cell. Biol. 20*, 4455−4461.
28. Westerheide, S. D., and Boss, J. M. (1999) Orientation and positional mapping of the subunits of the multicomponent transcription factors RFX and X2BP to the major histocompatibility complex class II transcriptional enhancer, *Nucleic Acids Res. 27*, 1635−1641.
29. Burd, A. L., Ingraham, R. H., Goldrick, S. E., Kroe, R. R., Crute, J. J., and Grygon, C. A. (2004) Assembly of major histocompatability complex (MHC) class II transcription factors: association and promoter recognition of RFX proteins, *Biochemistry 43*, 12750−12760.
30. Nagarajan, U. M., Long, A. B., Harreman, M. T., Corbett, A. H., and Boss, J. M. (2004) A hierarchy of nuclear localization signals governs the import of the regulatory factor X complex subunits and MHC class II expression, *J. Immunol. 173*, 410−419.
31. Muhlethaler-Mottet, A., Krawczyk, M., Masternak, K., Spilianakis, C., Kretsovali, A., Papamatheakis, J., and Reith, W. (2004) The S box of major histocompatibility complex class II promoters is a key determinant for recruitment of the transcriptional co-activator CIITA, *J. Biol. Chem. 279*, 40529−40535.
32. Masternak, K., Peyraud, N., Krawczyk, M., Barras, E., and Reith, W. (2003) Chromatin remodeling and extragenic transcription at the MHC class II locus control region, *Nat. Immunol. 4*, 132−137.
33. Krawczyk, M., Peyraud, N., Rybtsova, N., Masternak, K., Bucher, P., Barras, E., and Reith, W. (2004) Long distance control of MHC class II expression by multiple distal enhancers regulated by regulatory factor X complex and CIITA, *J. Immunol. 173*, 6200−6210.
34. Gomez, J. A., Majumder, P., Nagarajan, U. M., and Boss, J. M. (2005) X box-like sequences in the MHC class II region maintain regulatory function, *J. Immunol. 175*, 1030−1040.
35. Pace, C. N., Vajdos, F., Fee, L., Grimsley, G., and Gray, T. (1995) How to measure and predict the molar absorption coefficient of a protein, *Protein Sci. 4*, 2411−2423.
36. Laue, T. M., Shah, B. D., Ridgeway, T. M., and Pelletier, S. L. (1992) in *Analytical Ultracentrifugation in Biochemistry and Polymer Science* (Harding, S. E., Rowe, A. J. and Horton, J. C., Eds.) pp 90−125, The Royal Society of Chemistry, Cambridge, U.K.
37. Johnson, M. L., and Faunt, L. M. (1992) Parameter estimation by least-squares methods, *Methods Enzymol. 210*, 1−37.
38. Folta-Stogniew, E., and Williams, K. R. (1999) Determination of molecular masses of proteins in solution: implementation of an HPLC size exclusion chromatography and laser light scattering service in a core laboratory, *J. Biomol. Tech. 10*, 51−63.
39. Peretti, M., Villard, J., Barras, E., Zufferey, M., and Reith, W. (2001) Expression of the three human major histocompatibility complex class II isotypes exhibits a differential dependence on the transcription factor RFXAP, *Mol. Cell. Biol. 21*, 5699−5709.
40. Blackwood, E. M., and Kadonaga, J. T. (1998) Going the distance: a current view of enhancer action, *Science 281*, 60−63.
41. Long, A. B., Ferguson, A. M., Majumder, P., Nagarajan, U. M., and Boss, J. M. (2006) Conserved residues of the bare lymphocyte syndrome transcription factor RFXAP determine coordinate MHC class II expression, *Mol. Immunol. 43*, 395−409.

BI6023868